



Cite this: *New J. Chem.*, 2019, 43, 18805

Received 29th June 2019,
Accepted 4th November 2019

DOI: 10.1039/c9nj03391b

rsc.li/njc

Synthesis, characterization and photodynamic activity of Sn(IV) triarylcorroles with red-shifted Q bands†

Balaji Babu,^a Earl Prinsloo,^b John Mack^{ib*} and Tebello Nyokong^{id}^a

Two Sn(IV) triarylcorroles were synthesised and characterized. The absorption spectrum of a *meso*-thien-2-yl substituted tin(IV)corrole (**1-Sn**) is red shifted compared to its phenyl analogue (**2-Sn**) and shows no sign of aggregation in solution. **1-Sn** and **2-Sn** exhibited singlet oxygen quantum yields of 0.87 and 0.54 in DMF, and have a triplet lifetime of 31 and 50 μ s, respectively. Time dependent cellular uptake in MCF-7 cells for **1-Sn** reached a peak at 24 h, and **1-Sn** was found to be more lipophilic than **2-Sn**. **1-Sn** showed good photo-cytotoxicity on exposure to a Thorlabs 625 nm LED with an IC₅₀ value of 3.2 μ M and remained inactive in the dark.

Introduction

Photofrin[®] is an oligomeric mixture of porphyrins which is clinically approved for use as a photosensitizer dye for the photodynamic therapy (PDT) treatment of several different types of cancer.^{1–3} Photofrin[®] exerts its PDT effect by producing highly active ¹O₂.^{4–9} Although Photofrin[®] is an effective PDT agent, it has several drawbacks like prolonged skin photosensitivity and relatively weak absorption in the longer wavelength region. To overcome the drawbacks of Photofrin[®], various strategies have been pursued to form structurally modified porphyrins through modifications at the *meso*- and *beta*-positions.^{10–12} Corroles are macrocyclic aromatic (18 π electron) compounds which lack one *meso* carbon compared to porphyrins,^{13,14} and hence have contracted structures with three inner NH protons. Because of the steric hindrance between the three inner NH protons, the pyrrole rings of corroles do not remain coplanar. Corrole ligands are electron rich and have been found to stabilize high valent transition metal ions.^{15–18} Because of their unique structure and electronic properties, corroles and metal corroles have found applications in different fields. Corroles have higher molar extinction coefficients than porphyrins at the red end of the visible region. Free base corroles are less stable towards air and light because of their electron-rich nature.^{19–22} Incorporating electron withdrawing moieties at the *meso*-carbon or metallation with high valent metals improves their stability.

In a similar manner to porphyrins, corroles and metal corroles have been demonstrated to be favourable PDT agents which is primarily due to their relatively intense absorption in the Q band region, red shifting of absorption bands and capability of generating singlet oxygen.^{23–25} In particular, the PDT activity of gallium, phosphorus, aluminium and gold complexes of corrole has been studied extensively by different groups.^{26–29} The cytotoxicity in most cases is due to photo-generation of singlet oxygen which causes apoptotic cell death.²³ But in some instances metallation leads to a decrease in photocytotoxicity because of inefficient quenching of triplet state by molecular oxygen to produce singlet oxygen.²⁷

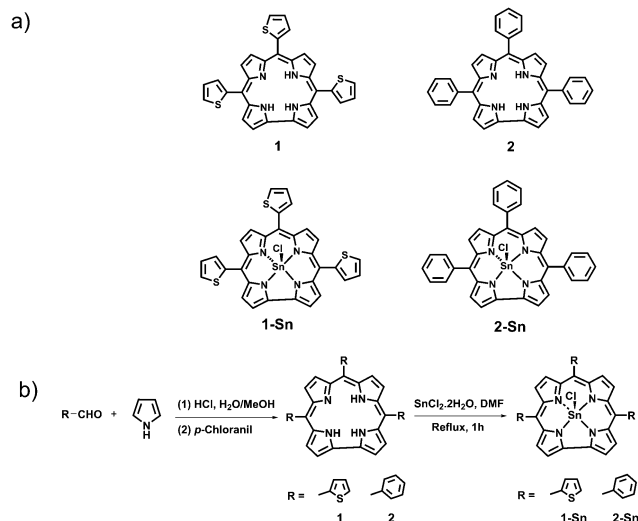
Considerable progress has been achieved in PDT research by exploring the PDT activity of different free base and metal corroles, such as Ga(III) complexes. To the best of our knowledge, only a few photocytotoxic studies have been carried out for Sn(IV) corroles.^{30–35} Many organotin complexes have been reported to have favourable antiproliferative and anti-tumor activity which induces the apoptotic process of cancer cell death.^{36,37} Incorporation of a central tin ion facilitates energy transfer from the singlet to the triplet manifold due to the heavy atom effect.^{38–40} We recently reported that a Sn(IV) tetraarylporphyrin complex with five-membered thien-2-yl moieties at the *meso*-positions showed remarkable PDT activity when irradiated with a Thorlabs 625 nm light emitting diode (LED).⁴¹ The thien-2-yl group enables a red shift of the main spectral bands towards the NIR region where there is deeper penetration of light into tissue.

In this study, we report the preparation of a novel Sn(IV) tris-thien-2-ylcorrole **1-Sn** (Scheme 1) through facile synthetic procedures that can be readily scaled up. Corrole ligands are known to absorb more intensely than porphyrins in the Q band

^a Institute for Nanotechnology Innovation, Department of Chemistry, Rhodes University, Makhanda 6140, South Africa. E-mail: j.mack@ru.ac.za

^b Biotechnology Innovation Centre, Rhodes University, Makhanda 6140, South Africa

† Electronic supplementary information (ESI) available. See DOI: 10.1039/c9nj03391b



Scheme 1 Molecular structures of the two sets of triarylcorroles that are investigated in this study.

region due to their lower symmetry,¹³ so the main goal of the study is to assess whether Sn(IV) tris(thien-2-yl)corroles provide superior PDT properties than their tetrathienylporphyrin counterparts. A tris(phenyl)corrole control compound (**2-Sn**) was prepared to explore the role of the thien-2-yl moiety. The photophysical and singlet oxygen generation properties of **1-Sn** and **2-Sn** have been compared along with their photodynamic therapy efficacy in MCF-7 cancer cells.

Results and discussion

Synthesis and structural characterization

The free base 5,10,15-tris(thien-2-yl)corrole (**1**) and 5,10,15-tris(phenyl)corrole (**2**) compounds were prepared by following the reported literature procedure.⁴² Briefly, the corresponding aldehyde (2 mol) and pyrrole (4 mol) were dissolved in MeOH/water (1:1 v/v), and the reaction was initiated by dilute HCl with further oxidation by *p*-chloranil to provide the crude product. The free base triarylcorroles (**1** and **2**) were obtained as green crystalline solids after purification by column chromatography. The corroles (**1** and **2**) were metallated with a Sn(IV) ion by refluxing the corroles with SnCl₂·2H₂O in DMF for 1 h.³¹ The solvent was evaporated, and the crude product was purified by flash chromatography to yield green crystalline Sn(IV) triarylcorroles (**1-Sn** and **2-Sn**) in good yield. The synthesized **1-Sn** and **2-Sn** complexes were characterized by standard techniques including ¹H-NMR spectroscopy and MALDI-TOF MS. The MALDI-TOF analyses of Sn(IV) triarylcorroles readily identified peaks corresponding to [M + H] and [M-Cl + H] (Fig. S1 and S2, see the ESI[†]).

Photophysical properties

The absorption spectra of free base corroles **1** and **2** and Sn(IV) triarylcorroles **1-Sn** and **2-Sn** in DMF are shown in Fig. 1. The molar extinction coefficients of the compounds are provided in Table 1.

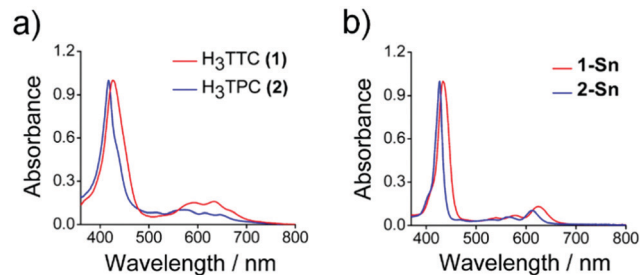


Fig. 1 UV-visible absorption spectra of (a) free base triarylcorroles **1** and **2**, and (b) the Sn(IV) complexes **1-Sn** and **2-Sn** in DMF.

Corroles are macrocyclic compounds similar to porphyrins with one less *meso*-carbon atom on the inner ligand perimeter. Their absorption spectra resemble those of porphyrins with slight differences.¹³ **1** and **2** have intense Soret bands at *ca.* 430 nm and broad intensified Q bands between 590 and 650 nm (Fig. 1a). The tin complexes (**1-Sn**, **2-Sn**) have more intense Soret bands than the free base compounds and narrow and relatively intense Q-bands (Fig. 1b). The absorption maximum of the Q-band of **1-Sn** lies at 627 nm, which is red-shifted by 14 nm relative to that of the analogous thien-2-yl porphyrin Sn(TTP) ($\lambda_{\max} = 613$ nm).⁴¹

1, **2**, **1-Sn** and **2-Sn** were found to be emissive, so the fluorescent spectra were studied in DMF (Fig. 2). The emission maxima and the fluorescence quantum yield values are summarized in Table 1. As expected the tin complexes are only weakly fluorescent with $\Phi_F \leq 0.01$ when excited at their Soret band maxima. The free base corroles emit in the 660–680 nm range, while the emission bands of the tin complexes are blue shifted (Fig. S3, see the ESI[†]). **1** has a lower Φ_F value (0.03) than the tris(phenyl) corrole **2** (0.10), due to the presence of heavy atom sulfur which quenches the excited singlet state by transferring energy to the triplet state.³⁸ Metallation with heavy metals usually reduces the Φ_F value because of the heavy atom effect.^{38,39} In accordance with this, the Φ_F values of **1-Sn** and **2-Sn** are much lower than those of free base corroles **1** and **2**. The fluorescence lifetime (τ_F) values at room temperature in DMF are summarized in Table 1. The fluorescence decay curves of all corroles at emission peaks upon photoexcitation at the Soret band maxima are provided in the ESI[†] (Fig. S4). The transient absorption curve of **1-Sn** and **2-Sn** was recorded in DMF (Fig. S5, see the ESI[†]) and triplet state lifetimes of 31 and 50 μ s were obtained for **1-Sn** and **2-Sn**, respectively, in N₂ gas saturated DMF solution.

The aggregation behavior of the free base and Sn(IV) corroles was investigated in DMF by measuring absorption spectra at different concentrations (0.78–25 μ M) (Fig. 3). Fig. 3 shows that there is no appearance of a new spectral band and also no broadening of any band observed in the concentration range studied. The linearity observed by plotting the Soret band absorption intensity against concentration shows that Sn(IV) corroles obey the Beer–Lambert law (inset of Fig. 3). The results show that the Sn(IV) corroles do not aggregate and remain monomeric which is one of the requirements for an effective

Table 1 Photophysical properties of free base (**1**, **2**) and Sn(IV) corroles (**1-Sn**, **2-Sn**) in DMF

	λ_{max} (nm) [ϵ , $10^4 \text{ M}^{-1} \text{ cm}^{-1}$]	λ_{em}^a (nm)	Φ_{F}^b	Φ_{Δ}^c	τ_{f} (ns)	τ_{T} (μs)
H ₃ TTC, 1	433 (6.75), 592 (0.85), 645 (1.16)	676	0.03	0.38	4.2	—
H ₃ TPC, 2	426 (3.46), 587 (0.59), 642 (0.63)	668	0.10	0.14	7.8	—
[Sn(IV)(TTC)Cl] 1-Sn	434 (9.58), 580 (0.61), 627 (1.15)	660	< 0.01	0.87	1.4	31
[Sn(IV)(TPC)Cl] 2-Sn	426 (10.02), 565 (0.45), 617 (0.83)	634	0.01	0.54	4.8	50

^a Excited at the Soret band. ^b ZnTPP as standard. ^c Rose Bengal as standard.

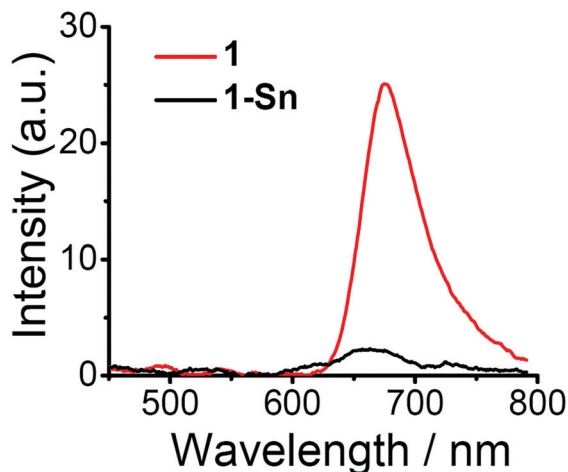


Fig. 2 Emission spectra of free base triarylcorrole **1** and the Sn(IV) complex **1-Sn** in DMF with the λ_{ex} value set at the Soret band maximum.

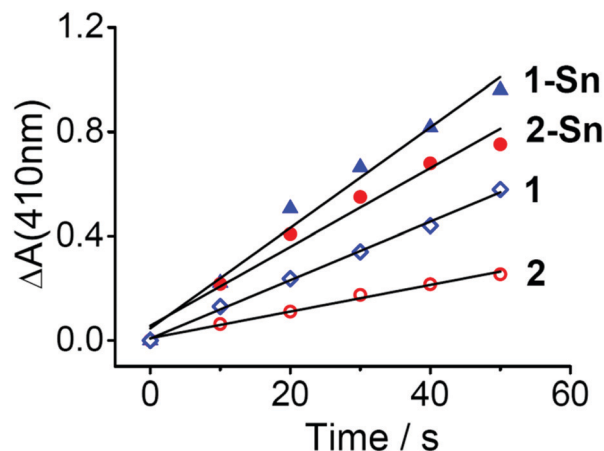


Fig. 4 Plot of the change in absorbance of DPBF at 410 nm vs. irradiation time in the presence of **1**, **2**, **1-Sn** and **2-Sn** in DMF.

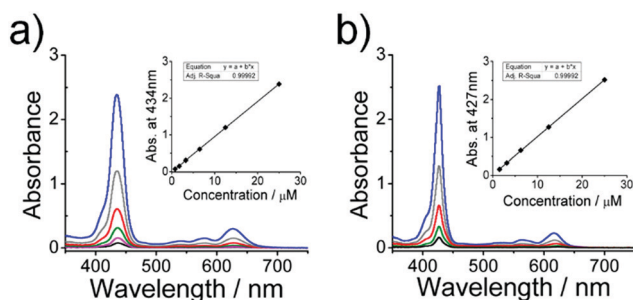


Fig. 3 UV-visible absorption spectra of (a) **1-Sn** and (b) **2-Sn** at different concentrations in DMF. The inset plots show the Soret-band absorbance vs. concentration of the metal corroles.

PDT agent.⁴ Aggregation of PDT drugs has been found to minimize the PDT efficacy.

Singlet oxygen quantum yields

To be an effective PDT agent, the photosensitizer should be able to produce reactive oxygen species (ROS) such as $^1\text{O}_2$ and $\cdot\text{OH}$ on exposure to a specific wavelength of light.⁴ The ability of **1**, **2**, **1-Sn**, and **2-Sn** to produce singlet oxygen is measured by the scavenger method with DPBF (1,3-diphenylisobenzofuran) in DMF using Rose Bengal as the standard. DPBF absorbs at 418 nm and reacts with $^1\text{O}_2$ to form 1,2-dibenzoylbenzene which does not absorb in the visible region. The decrease in DPBF absorption at 410 nm ($\Delta A_{410\text{nm}}$) is directly proportional to the amount of $^1\text{O}_2$ generated.⁴³ As shown in Fig. 4,

the absorbance of DPBF decreased linearly with increasing illumination time (0–50 s) in the presence of each complex. The singlet oxygen quantum yields (Φ_{Δ}) are calculated by comparing the slopes of the lines for the complex and the standard (Table 1). Tristhien-2-ylcorrole **1** has a Φ_{Δ} value of 0.38, which is significantly higher than that of its phenyl analogue **2** ($\Phi_{\Delta} = 0.14$), due to the heavy atom effect associated with the thienyl sulfur atoms. The singlet oxygen quantum yields of the Sn(IV) corroles are higher than those of the free base dyes due to the incorporation of the heavy central atom.

A very high Φ_{Δ} value of 0.87 is observed for **1-Sn** suggesting that **1-Sn** can be used as a photosensitizer during the photodynamic therapy of cancer. Incorporation of a heavy Sn(IV) ion increases the Φ_{Δ} value almost two-fold. The heavy atom effect facilitates energy transfer from the S_1 to the T_1 manifold which can then be further transferred to molecular oxygen to form $^1\text{O}_2$.^{43,44} Sn(IV) tristhien-2-ylcorrole **1-Sn** has a higher Φ_{Δ} value than its Sn(IV) tetrathienylporphyrin ($\Phi_{\Delta} = 0.83$) counterpart.⁴¹ When irradiation was carried out in the presence of a singlet oxygen quencher such as NaN_3 , there was a large decrease in the $\Delta A_{410\text{nm}}$ values (Fig. S6, see ESI†). In contrast, the presence of a hydroxyl quencher such as DMSO has no apparent effect on the $^1\text{O}_2$ generation measurement. Further control experiments in the dark and with DPBF alone demonstrated that **1**, **2**, **1-Sn** and **2-Sn** failed to produce $^1\text{O}_2$ in these contexts. The results of all these experiments suggest that $^1\text{O}_2$ is the only significant ROS that is produced on exposure to suitable light irradiation.

Lipophilicity by the shake-flask method

The cellular uptake of the free base corroles and their tin complexes depends on their lipophilicity ($\log P$). The lipophilicity of **1**, **2**, **1-Sn** and **2-Sn** was measured by the shake flask method (Table 2).⁴⁵ The $\log P$ value of **1-Sn** is slightly higher than that of **2-Sn**, so **1-Sn** is more lipophilic than **2-Sn**. Similarly, free base **1** is more lipophilic than **2**. Moderately lipophilic dye compounds are known to easily pass through the lipid bilayer of cells and tend to localise inside the cells and display significant PDT activity.⁴⁶

Cellular uptake

The cellular uptake of the Sn(IV) triarylcorroles was examined by incubating the MCF-7 cells with Sn(IV) corroles (10 μM) for 12, 24 and 48 h. The fluorescence intensity of the internalized Sn(IV) corroles was measured. Fig. 5 shows that cellular uptake of the Sn(IV) triarylcorroles reached a peak at 24 h. Cellular uptake of **1-Sn** at 24 h is 2-fold higher than its phenyl analogue **2-Sn** and this is in accordance with the order of lipophilicity.

Cytotoxicity assays

The high Φ_{Δ} values that were determined for the Sn(IV) triarylcorroles (**1-Sn** and **2-Sn**) prompted us to perform PDT activity experiments in MCF-7 cancer cells. The cytotoxicity of free base and Sn(IV) corroles with/without illumination against MCF-7 cell lines was evaluated by MTT assay.⁴⁷ The MCF-7 cells were incubated with different concentrations of **1**, **2**, **1-Sn** and **2-Sn** (0.78–50 μM) for 24 h and irradiated with 625 nm laser light for 30 min. Dark controls were used to measure the PDT effect. The extent of cytotoxicity of all the compounds was measured from the IC_{50} value which is given in Table 3 along with two related compounds. A comparison of the MTT assay data is given in Fig. 6a and b. **1-Sn** and **2-Sn** remain non-toxic in the dark over most of the concentration range studied. Photo-irradiation with

Table 2 Lipophilicity ($\log P_{\text{O/W}}$) of the compounds studied^a

	$\log P_{\text{O/W}}$
1	1.56 \pm 0.09
2	1.41 \pm 0.05
1-Sn	1.33 \pm 0.04
2-Sn	1.24 \pm 0.03

^a By the shake flask method.⁴⁵

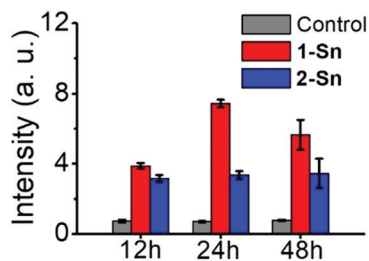


Fig. 5 Time-dependent cellular uptake of Sn(IV) corroles into MCF-7 cells from solutions as measured by fluorescence intensity using excitation and emission wavelengths of 422 and 650 nm, respectively.

Table 3 Cytotoxicity and photocytotoxicity data for **1**, **2**, **1-Sn**, **2-Sn**, Sn(IV)TTP(3PyO)₂ and its tetraphenyl analogue (Sn(IV)TPP(3PyO)₂) towards the MCF-7 cell line

	IC_{50} (μM) Dark ^a	IC_{50} (μM) Light ^b	IC_{50} (μM) Light + NAC
1	> 50	> 50	> 50
2	> 50	> 50	> 50
1-Sn	> 50	3.2 (\pm 0.1)	> 50
2-Sn	> 50	13.1 (\pm 0.2)	> 50
[Sn(IV)TTP(3PyO) ₂] ^c	> 50	5.6 (\pm 1.1)	—
[Sn(IV)TPP(3PyO) ₂] ^c	> 50	18.7 (\pm 1.1)	—

^a The IC_{50} values correspond to 24 h incubation in the dark without any photoexposure. ^b The IC_{50} values correspond to 24 h incubation in the dark followed by photoexposure to a 625 nm laser (240 mW cm⁻²) for 30 min. ^c Ref. 41.

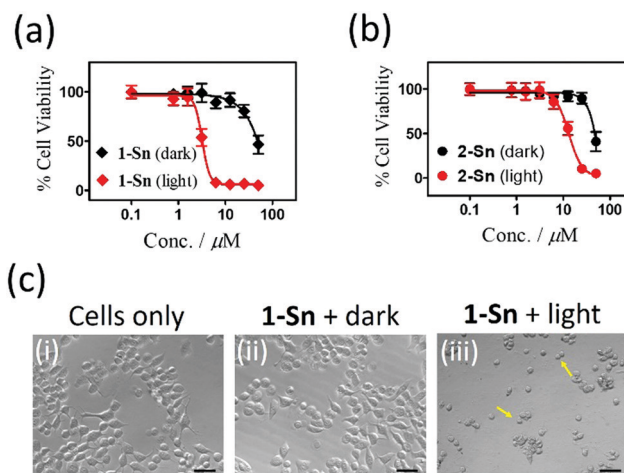


Fig. 6 Cytotoxicity of (a) **1-Sn** and (b) **2-Sn** in MCF-7 cells after 24 h incubation in the dark followed by photo-irradiation (30 min) with a Thorlabs 625 nm LED as determined by MTT assay. The dark treated cells are represented by solid black circles and photoexposed cells are represented by solid red circles. (c) Morphological changes observed in the MCF-7 cells by inverted microscopy, (i) control cells, (ii) **1-Sn** (10 μM) treated cells kept in the dark, and (iii) **1-Sn** (10 μM) treated cells after photoirradiation with 625 nm LED light for 30 min [scale bar: 200 μm].

a Thorlabs 625 nm LED showed a significant enhancement in cytotoxicity. **1-Sn** showed a *ca.* 4-fold higher photocytotoxicity effect than its phenyl analogue **2-Sn**.

1-Sn and **2-Sn** have IC_{50} values of 3.2 and 13.1 μM , respectively, in MCF-7 cells. The significant enhancement in the photocytotoxicity of **1-Sn** compared to **2-Sn** is consistent with the singlet oxygen quantum yield and lipophilicity data. The photocytotoxicity of Sn(IV) triarylcorroles is hence enhanced by incorporating thien-2-yl rings. **1-Sn** was found to exhibit better photocytotoxicity than a Sn(IV) tetraphenylporphyrin with 3-pyridyloxy axial ligands (Sn(IV)TTP(3PyO)₂) that we reported recently, which had an IC_{50} value of 5.6 μM when MCF-7 cells were irradiated using the same experimental setup.⁴¹ When compared to the Sn(IV) corroles, the free base compounds exhibit much less dark cytotoxicity and photocytotoxicity. Free bases **1** and **2** remain inactive both in the dark and under light illumination over the concentration range studied

(Fig. S7, see ESI†). To demonstrate the involvement of ROS in photocytotoxicity of tin corroles, photo-irradiation was carried out in the presence of *N*-acetyl cysteine (NAC) as a ROS scavenger. In the presence of NAC, the photodynamic activity of the tin corroles was found to decrease significantly. This indicates that the photocytotoxicity of the Sn(IV) corroles is due to the generation of ROS upon photo-irradiation.

In order to further study its PDT activity, **1-Sn** (10 μM of a stock solution) was added to the MCF-7 cells, which were incubated for 24 h in the dark and were then illuminated with a 625 nm LED for 30 min (Fig. 6c). Inverted fluorescence microscopy images of light treated cells incubated with **1-Sn** show the morphological changes that occur such as cell shrinkage, loss of adherence and reduced cell density, which is consistent with apoptotic behaviour.⁴⁸ In contrast, no difference in cell morphology is observed between non-irradiated **1-Sn**-treated cells and the control cells (Fig. 6c). These results suggest that **1-Sn** is cytotoxic to MCF-7 cells only upon light irradiation and remains non-toxic in the dark at the concentration studied (10 μM) in this context. It is noteworthy that the IC_{50} value of 3.2 (± 0.1) μM for **1-Sn** in MCF-7 cells (Table 3) is comparable to those that have been reported for Photofrin[®] and Cisplatin of 1.0 (± 0.1)^{49a} and 2.0 (± 0.3)^{49b} μM , respectively.

Theoretical calculations

The red shift of the Q and B bands of **1-Sn** relative to those of **2-Sn** can be readily explained on the basis of theoretical calculations and a consideration of the effect that the *meso*-aryl groups have on the four frontier π -MOs of Michl's perimeter model⁵⁰ which are derived from the HOMO and LUMO of a $\text{C}_{15}\text{H}_{15}^{3-}$ parent hydrocarbon perimeter with $\Delta M_L = \pm 4$ and ± 5 angular nodal patterns, respectively. Michl's *a*, *s*, *-a* and *-s* labelling system is used depending on whether an angular nodal plane is aligned with the *y*-axis (Fig. 7).^{50,51} In the context of corroles, the absence of the four-fold symmetry of metalloporphyrins results in a significant lifting of the degeneracy of the *-a* and *-s* MOs for symmetry reasons (Fig. 7) and a mixing of the forbidden and allowed properties of the Q and B bands.⁵¹ A significant narrowing of the HOMO–LUMO gap is predicted (Fig. 7) due to the effect of replacing the phenyl rings of **2-Sn** with thien-2-yl rings, which leads to a predicted red shift in the TD-DFT spectra at the CAM-B3LYP/6-31G(d) basis sets (Fig. S8 and Table S1, see ESI†).

Experimental

Materials

Ultra-pure water was obtained from a Milli-Q Water System (Millipore Corp, Bedford, MA, USA). DMF and trypan blue were purchased from Sigma Aldrich. Cultures of the MCF-7 cells were obtained from Cellonex[®]. 10% (v/v) heat-inactivated fetal calf serum (FCS) and 100 units per mL penicillin–100 $\mu\text{g mL}^{-1}$ streptomycin–amphotericin B were obtained from Biowest[®]. Dulbecco's phosphate-buffered saline (DPBS) and Dulbecco's

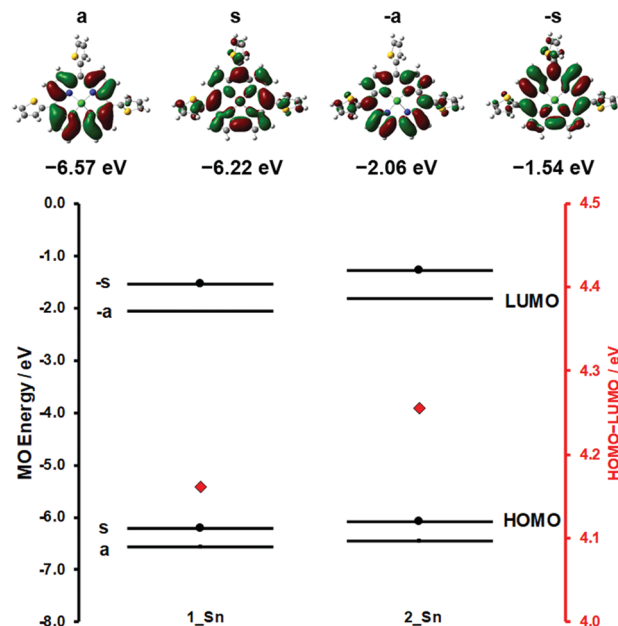


Fig. 7 The angular nodal patterns and MO energy values of the *a*, *s*, *-a* and *-s* MOs of **1-Sn** (TOP). MO energies for **1-Sn** and **2-Sn** at the CAM-B3LYP/SDD level of theory (BOTTOM). Occupied MOs are highlighted with small black squares and large red diamonds are used to denote the HOMO–LUMO band gaps and are plotted against a secondary axis. Black circles are used to highlight the *s* and *-s* MOs.

modified Eagle's medium (DMEM) were purchased from Lonza[®].

Equipment

UV-visible absorption spectra were measured on a Shimadzu UV-2550 spectrophotometer, while a Varian Eclipse spectrofluorimeter and a 360–1100 nm filter were used to record the fluorescence emission spectra. Fluorescence lifetimes were measured using a time-correlated single photon counting setup (TCSPC) (FluoTime 300, Picoquant GmbH) with a diode laser (LDH-P-670, Picoquant GmbH, 20 MHz repetition rate, 44 ps pulse width). Triplet state lifetimes were determined in nitrogen saturated DMF solutions at 500 nm using an Edinburgh Instruments LP980 spectrometer with a pump beam of 425 nm provided by an Ekspla NT-342B laser. MS data were collected on a Bruker[®] AutoFLEX III Smart-beam TOF/TOF mass spectrometer using α -cyano-4-hydroxycinnamic acid as the matrix in the positive ion mode.

Theoretical calculations

The Gaussian 09 software package⁵² was used to carry out DFT geometry optimizations for **1**, **2**, **1-Sn** and **2-Sn** by using the B3LYP functional with SDD basis sets. TD-DFT calculations were carried out with the CAM-B3LYP functional, since the inclusion of a long-range correction provides more accurate results when excited states have significant intramolecular charge transfer character as is likely to be the case with corroles. Simulated spectra were generated by using the Chemcraft program.⁵³

Lipophilicity: shake flask method

The cellular uptake of a compound through its ability to permeate into the biological membrane is closely related to its lipophilicity, which is defined here as the *n*-octanol/water partition coefficient (expressed in $\log P_{o/w}$). The $\log P_{o/w}$ values were determined in triplicate for the free base triarylcorroles and Sn(IV) complexes by the standard “shake-flask” method.⁴⁵ Since these compounds are insoluble in both 1-octanol and water, the partition coefficient was measured in CHCl₃-H₂O mixtures to derive $\log P_{\text{chloroform}}$ values and the $\log P_{\text{octanol}}$ values were derived using the equation $\log P_{\text{octanol}} = (1.343 + \log P_{\text{chloroform}})/1.126$.⁴⁵ To measure the $\log P_{\text{chloroform}}$ value, ca. 2 mg of the complex was dissolved in 10 mL of dry chloroform. 5 mL of the chloroform solution was added to 5 mL of Milli-Q water and stirred at room temperature for 4 h. The solution was kept still for 1 h to obtain two clear layers. Aliquots were taken from the chloroform layer, and an absorbance value was measured at the Soret band maximum for the chloroform layer (*A*) and also for the stock chloroform solution (*A*₀). To obtain the concentration of the compounds in the water layer, the difference in absorbance (*A*₀ - *A*) was calculated. From that, $\log P_{\text{chloroform}} = \log A_0 / \log(A_0 - A)$ was calculated along with $\log P_o$.

Cell culture studies – dark toxicity tests

Cultures of MCF-7 breast cancer cell lines were grown in Dulbecco's modified Eagle's medium (DMEM) containing l-glutamine and phenol red, and supplemented with 10% heat-inactivated fetal calf serum (FCS) and 100 units per mL penicillin-100 µg mL⁻¹ streptomycin-amphotericin B. The cells were grown in a T75 flask and were incubated at 37 °C under 5% CO₂, until a cell confluence of 80–100% was achieved. A fluorescence LED (FL-LED) inverted microscope was used to view the cells under phase contrast (Zeiss-AxioVert). The cells were then rinsed with Dulbecco's modified phosphate buffer saline (DPBS) and lifted using trypsin. The cells were counted using a hemocytometer through the addition of 50 µL of DPBS and cell culture (from a known volume) and 100 µL of trypan blue. Cells were seeded at a density of ca. 10 000 cells per well in 96-well tissue culture plates with 100 µL of supplemented DMEM containing phenol red and allowed to attach. The cells were then incubated at 37 °C under 5% CO₂ for 24 h. The attached cells were then rinsed with 100 µL of DPBS, and the studied compounds were added at different concentrations. Control cells were given fresh DMEM medium. The plates were re-incubated at 37 °C under 5% CO₂ in the dark for 24 h. Following this, the wells were rinsed with 100 µL of DPBS; the media were replaced with fresh media, and the cells were incubated overnight.

Photodynamic therapy tests

Photodynamic therapy effects were determined by incubating cells seeded in the manner described above with gradient concentrations of the compounds being studied in a 96-well

plate at a density of 10 000 cells per well in the culture medium (100 µL). The plate was incubated at 37 °C under 5% CO₂ in the dark for 24 h, and was then washed with 100 µL of DPBS and the medium was replaced with supplemented DMEM with no phenol red. The 96 well plate was irradiated for 30 min using the illumination kit of a Modulight[®] 7710–680 Medical Laser fitted with a Thorlab M625L3 light emitting diode that was found to provide an irradiance of 240 mW cm⁻² (measured using a Coherent FieldmaxII TOP energy/power meter fitted with a Coherent Powermax PM10 sensor) in this context. After irradiation, the medium was replaced with a fresh medium containing phenol red and incubated for 20 h in the dark. After the incubation period, 5 mg mL⁻¹ of MTT (20 µL) was added to each well and incubated for an additional 3 h. The culture medium was finally discarded, and 200 µL of DMSO was added to dissolve the formazan crystals. The absorbance at 540 nm was measured using a Molecular Devices Spectra Max M5 plate reader. Cytotoxicity of the complex was measured as the percentage ratio of the absorbance of the treated cells to the untreated controls. The IC₅₀ values were determined by non-linear regression analysis (GraphPad Prism 5).

To confirm photodynamic activity in the cancer cells, the morphological changes of the treated MCF-7 cells were monitored after illumination and in its absence. Approximately 1 × 10⁵ cells were seeded in a 24-well plate and allowed to grow for 24 h. **1-Sn** (10 µM) was added to each well. After 24 h incubation, cells were irradiated with a 625 nm LED for 30 min and incubated for 24 h. Some treated cells and control cells were kept in the dark. Morphological changes were observed using a Zeiss-AxioVert inverted microscope (Fig. 6).

Synthesis of precursors

5,10,15-Tris(thien-2-yl)corrole (H₃TTC) (**1**) and 5,10,15-trisphenylcorrole (H₃TPC) (**2**) were prepared according to literature procedures.^{42a} **1-Sn** and **2-Sn** were synthesized as described elsewhere.³⁰ Briefly, the appropriate triarylcorrole (0.5 mmol) and SnCl₂·2H₂O (5 mmol) were dissolved in a minimal volume of dry DMF (3 mL) and refluxed for 2 h. After cooling and purification by short flash column chromatography (Silica, CHCl₃) the product was obtained as a green solid in 70–80% yield.

5,10,15-Tris(thien-2-yl)corrole Sn(IV)-dichloride (1-Sn). ¹H NMR (CDCl₃, 600 MHz): δ (ppm) 9.44 (d, *J* = 4.62 Hz, 3H), 9.22 (d, *J* = 4.02 Hz, 2H), 9.06 (m, 3H), 8.05 (d, *J* = 3.18 Hz, 1H), 7.98 (d, *J* = 3.24 Hz, 2H), 7.90 (d, *J* = 5.4 Hz, 2H), 7.85 (d, *J* = 5.46 Hz, 1H), 7.57 (m, 2H), 7.52 (m, 1H). UV-Vis (DMF): λ_{max}/nm (ε/M⁻¹ cm⁻¹) 434 (95 830), 580 (6050), 627 (11 480). MS (MALDI-TOF): *m/z* for SnClC₃₁N₄S₃H₁₇, calculated: 695.93; found 696.69 [M + H]⁺, 661.69 [M-Cl + H].

5,10,15-Trisphenylcorrole Sn(IV)-dichloride (2-Sn)^{42b}. ¹H NMR (CDCl₃, 600 MHz): δ (ppm) 9.23 (d, *J* = 4.02 Hz, 2H), 9.15 (d, *J* = 4.62 Hz, 2H), 8.85 (m, 4H), 8.31 (d, *J* = 6.96 Hz, 2H), 7.95 (m, 4H), 7.83 (m, 9H). UV-Vis (DMF): λ_{max}/nm (ε/M⁻¹ cm⁻¹) 426 (100 180), 565 (4480), 617 (8280). MS (MALDI-TOF): *m/z* for SnClC₃₇N₄H₂₃, calculated: 678.06; 678.71 [M + H]⁺, 643.68 [M-Cl + H].

Conclusions

In conclusion, two Sn(IV) corroles with thien-2-yl and phenyl substituents at *meso*-positions were synthesised and characterized. The partial lifting of the forbidden nature of the Q bands of triarylcorroles⁵¹ makes these dyes more suitable for use in applications that depend on light absorption at the red end of the visible region than their tetraarylporphyrin analogues. The thien-2-yl appended Sn(IV) triarylcorrole (**1-Sn**) has a significantly more red-shifted lower energy Q band than its phenyl analogue which enhances its absorption on the edge of the therapeutic window. The Sn(IV) triarylcorroles **1-Sn** and **2-Sn** have significantly higher Φ_{Δ} quantum yields than the corresponding free bases due to the heavy atom effect associated with the central metal ion. **1-Sn** which bears thien-2-yl rings was found to be highly photocytotoxic against MCF-7 cancer cells while remaining significantly less toxic in the dark. The Sn(IV) trithienylcorrole exhibited enhanced photocytotoxicity during *in vitro* studies with MCF-7 cells than its Sn(IV) tetrathienylporphyrin counterpart,⁴¹ and exhibits a similar lack of aggregation in polar solvents despite having only one axial ligand. The light *versus* dark cytotoxicity profiles for **1-Sn** demonstrate that further in depth study of Sn(IV) trithienylcorroles is merited, since their axial ligation could be further modified to enhance drug transport and cell targeting and their relatively facile synthesis makes them good candidates for scale up as a commercial photosensitizer dyes for PDT.

Conflicts of interest

There are no conflicts of interest to declare.

Acknowledgements

This work was supported by the Department of Science and Technology (DST) and National Research Foundation (NRF) of South Africa through DST/NRF South African Research Chairs Initiative for Professor of Medicinal Chemistry and Nanotechnology (uid: 62620). Photophysical measurements were made possible by the Laser Rental Pool Programme of the Council for Scientific and Industrial Research (CSIR) of South Africa. Theoretical calculations were carried out at the Centre for High Performance Computing in Cape Town.

References

- 1 D. E. Dolmans, D. Fukumura and R. K. Jain, *Nat. Rev. Cancer*, 2003, **3**, 380.
- 2 M. Wainwright, *Chem. Soc. Rev.*, 1996, **25**, 351.
- 3 T. J. Dougherty and J. G. Levy, in *Biomedical Photonics Handbook*, ed. T. Vo-Dinh, CRC Press, New York, 2003, p. 38-1.
- 4 M. Ethirajan, Y. Chen, P. Joshi and R. K. Pandey, *Chem. Soc. Rev.*, 2011, **40**, 340.
- 5 (a) P. R. Ogilby, *Chem. Soc. Rev.*, 2010, **39**, 3181; (b) B. Habermeyer and R. Guillard, *Photochem. Photobiol. Sci.*, 2018, **17**, 1675.
- 6 A. B. Ormond and H. S. Freeman, *Materials*, 2013, **6**, 817.
- 7 J. P. Celli, B. Q. Spring, I. Rizvi, C. L. Evans, K. S. Samkoe, S. Verma, B. W. Pogue and T. Hasan, *Chem. Rev.*, 2010, **110**, 2795.
- 8 K. Plaetzer, B. Krammer, J. Berlanda, F. Berr and T. Kiesslich, *Lasers Med. Sci.*, 2009, **24**, 259.
- 9 I. Yoon, J. Z. Li and Y. K. Shim, *Clin. Endosc.*, 2013, **46**, 7.
- 10 M. Luciano and C. Brückner, *Molecules*, 2017, **22**, 980.
- 11 R. Paolesse, S. Nardis, D. Monti, M. Stefanelli and C. Di Natale, *Chem. Rev.*, 2017, **117**, 2517.
- 12 M. Kielmann, C. Prior and M. O. Senge, *New J. Chem.*, 2018, **42**, 7529.
- 13 J. F. B. Barata, M. G. P. M. S. Neves, M. A. F. Faustino, A. C. Tomé and J. A. S. Cavaleiro, *Chem. Rev.*, 2017, **117**, 3192.
- 14 I. Aviv and Z. Gross, *Chem. Commun.*, 2007, 1987.
- 15 I. Aviv-Harel and Z. Gross, *Coord. Chem. Rev.*, 2011, **255**, 717.
- 16 F. B. Barata, M. G. P. M. S. Neves, M. A. F. Faustino, A. C. Tome and J. A. S. Cavaleiro, *Chem. Rev.*, 2016, **117**, 3192.
- 17 S. Nardis, F. Mandoj, M. Stefanelli and R. Paolesse, *Coord. Chem. Rev.*, 2019, **388**, 360.
- 18 G. Pomarico, D. Monti, M. Bischetti, A. Savoldelli, F. R. Fronczek, K. M. Smith, D. Genovese, L. Prodi and R. Paolesse, *Chem. – Eur. J.*, 2018, **24**, 8438.
- 19 T. Ding, E. A. Alema, D. A. Modarelli and C. J. Ziegler, *J. Phys. Chem. A*, 2005, **109**, 7411.
- 20 C. P. Gros, J.-M. Barbe, E. Espinoza and R. Guillard, *Angew. Chem., Int. Ed.*, 2006, **45**, 5642.
- 21 G. R. Geier III, J. F. B. Chick, J. B. Callinan, C. G. Reid and W. P. Auguscinski, *J. Org. Chem.*, 2004, **69**, 4159.
- 22 C. Tardieux, C. P. Gros and R. Guillard, *J. Heterocycl. Chem.*, 1998, **35**, 965.
- 23 A. Mahammed and Z. Gross, *Coord. Chem. Rev.*, 2019, **379**, 121.
- 24 Z. Zhang, H. H. Wang, H. J. Yu, Y. Z. Xiong, H. T. Zhang, L. N. Ji and H. Y. Liu, *Dalton Trans.*, 2017, **46**, 9481.
- 25 B. Ventura, A. Degli Esposti, B. Koszarna, D. T. Gryko and L. Flamigni, *New J. Chem.*, 2005, **29**, 1559.
- 26 (a) X. Liang, J. Mack, L.-M. Zheng, Z. Shen and N. Kobayashi, *Inorg. Chem.*, 2014, **53**, 2797; (b) Z. Zhang, H. J. Yu, H. Huang, H. H. Wang, S. Wu, H. Y. Liu and H. T. Zhang, *Eur. J. Med. Chem.*, 2019, **163**, 779; (c) Y. G. Wang, Z. Zhang, H. Wang and H. Y. Liu, *Bioorg. Chem.*, 2016, **67**, 57.
- 27 (a) H. Agadjanian, J. Ma, A. Rentsendorj, V. Valluripalli, J. Y. Hwang, A. Mahammed, D. L. Farkas, H. B. Gray, Z. Gross and L. K. Medina-Kauwe, *Proc. Natl. Acad. Sci. U. S. A.*, 2009, **106**, 6105; (b) A. Mahammed, H. B. Gray, J. J. Weaver, K. Sorasaene and Z. Gross, *Bioconjugate Chem.*, 2004, **15**, 738; (c) F. Cheng, L. T. Huang, H. H. Wang, Y. J. Liu, J. Kandhadi, H. Wang, L. N. Ji and H. Y. Liu, *Chin. J. Chem.*, 2017, **35**, 86; (d) P. Lim, A. Mahammed, Z. Okun, I. Saltsman, Z. Gross, H. B. Gray and J. Termini, *Chem. Res. Toxicol.*, 2012, **25**, 400; (e) Z. Ye, Y. Liang, Y. Ma, B. Lin, L. Cao, B. Wang, Z. Zhang, H. Yu, J. Li, M. Huang, K. Zhou, Q. Zhang, X. Liu and J. Zeng, *Cancer Med.*, 2018, **7**, 3057; (f) Z. Zhang, J. Y. Wen, B. B. Lv, X. Li, X. Ying, Y. J. Wang,

- H. T. Zhang, H. Wang, H. Y. Liu and C. K. Chang, *Appl. Organomet. Chem.*, 2016, **30**, 132; (g) Z. Y. Ye, Y. F. Liang, Y. Ma, B. H. Lin, L. B. Cao, B. Wang, Z. Zhang, H. B. Yu, J. X. Li, M. Y. Huang, K. Y. Zhou, Q. Z. Zhang, X. G. Liu and J. C. Zeng, *Cancer Med.*, 2018, **7**, 3057.
- 28 (a) P. Lim, A. Mahammed, Z. Okun, I. Saltsman, Z. Gross, H. B. Gray and J. Termini, *Chem. Res. Toxicol.*, 2012, **25**, 400; (b) X. Liu, A. Mahammed, U. Tripathy, Z. Gross and R. P. Steer, *Chem. Phys. Lett.*, 2008, **459**, 113; (c) G. Pomarico, S. Nardis, M. L. Naitana, M. G. H. Vicente, K. M. Kadish, P. Chen, L. Prodi, D. Genovese and R. Paolesse, *Inorg. Chem.*, 2013, **52**, 4061.
- 29 (a) R. D. Teo, H. B. Gray, P. Lim, J. Termini, E. Domeshek and Z. Gross, *Chem. Commun.*, 2014, **50**, 13789; (b) A. B. Alemayehu, N. U. Day, T. Mani, A. B. Rudine, K. E. Thomas, O. A. Gederaas, S. A. Vinogradov, C. C. Wamser and A. Ghosh, *ACS Appl. Mater. Interfaces*, 2016, **8**, 18935.
- 30 L. Simkhovich, A. Mahammed, I. Goldberg and Z. Gross, *Chem. – Eur. J.*, 2001, **7**, 1041.
- 31 W. Sinha, M. Kumar, A. Garai, C. S. Purokit, T. Som and S. Kar, *Dalton Trans.*, 2014, **43**, 12564.
- 32 A. N. Xie, Z. Zhang, H. H. Wang, A. Ali, D. X. Zhang, H. Wang, L. N. Ji and H. Y. Liu, *J. Porphyrins phthalocyanines*, 2018, **22**, 739.
- 33 K. M. Kadish, S. Will, V. A. Adamian, B. Walther, C. Erben, Z. Ou, N. Guo and E. Vogel, *Inorg. Chem.*, 1998, **37**, 4573.
- 34 L. Wagnert, A. Berg, E. Stavitski, T. Berthold, G. Kothe, I. Goldberg, A. Mahammed, L. Simkhovich, Z. Gross and H. Levanon, *Appl. Magn. Reson.*, 2006, **30**, 591.
- 35 O. G. Tsay, B.-K. Kim, T. L. Lu, J. Kwak and D. G. Churchill, *Inorg. Chem.*, 2013, **52**, 1991.
- 36 S. K. Hadjidakou and N. Hadjiliadis, *Coord. Chem. Rev.*, 2009, **253**, 235.
- 37 C. N. Banti, S. K. Hadjidakou, T. Sismanoglu and N. Hadjiliadis, *J. Inorg. Biochem.*, 2019, **194**, 114.
- 38 E. Pomarico, P. Pospíšil, M. E. F. Bouduban, J. Vestfrid, Z. Gross, Z. S. Zálíš, M. Chergui and A. Vlček, *J. Phys. Chem. A*, 2018, **122**, 7256.
- 39 J. Vestfrid, M. Botoshansky, J. H. Palmer, A. C. Durrell, H. B. Gray and Z. Gross, *J. Am. Chem. Soc.*, 2011, **133**, 12899.
- 40 J. Vestfrid, I. Goldberg and Z. Gross, *Inorg. Chem.*, 2014, **53**, 10536.
- 41 B. Babu, E. Amuhaya, D. Oluwole, E. Prinsloo, J. Mack and T. Nyokong, *Med. Chem. Commun.*, 2019, **10**, 41.
- 42 (a) B. Kozarna and D. T. Gryko, *J. Org. Chem.*, 2006, **71**, 3707; (b) L. Yun, H. Vazquez-Lima, H. Fang, Z. Yao, G. Geisberger, C. Dietl, A. Ghosh, P. J. Brothers and X. Fu, *Inorg. Chem.*, 2014, **53**, 7047.
- 43 S. Dumas, J. C. Lepretre, A. Lepellec, A. Darmanyan and P. Jardon, *J. Photochem. Photobiol., A*, 2004, **163**, 97.
- 44 (a) R. Bonnett and G. Martínez, *Tetrahedron*, 2001, **57**, 9513; (b) J. D. Spikes and J. C. Bommer, *Photochem. Photobiol.*, 1993, **58**, 346.
- 45 (a) C. Hansch, P. P. Maloney, T. Fujita and R. Muir, *Nature*, 1962, **194**, 178; (b) T. Fujita, J. Iwasa and C. Hansch, *J. Am. Chem. Soc.*, 1964, **86**, 5175.
- 46 (a) A. M. Odeh, J. D. Craik, R. Ezzeddine, A. Tovmasyan, I. Batinic-Haberle and L. T. Benov, *PLoS One*, 2014, **9**, e108238; (b) A. Tovmasyan, N. Babayan, D. Poghosyan, K. Margaryan, B. Harutyunyan and R. Grigoryan, *J. Inorg. Biochem.*, 2014, **140**, 94; (c) R. Ezzeddine, A. Al-Banaw, A. Tovmasyan, J. D. Craik, I. Batinic-Haberle and L. T. Benov, *J. Biol. Chem.*, 2013, **288**, 36579.
- 47 M. V. Berridge, P. M. Herst and A. S. Tan, *Biotechnol. Annu. Rev.*, 2005, **11**, 127.
- 48 (a) W. Lieberthal, J. S. Koh and J. S. Levine, *Semin. Nephrol.*, 1998, **18**, 505; (b) L. R. Comini, I. M. Fernandez, N. B. R. Vittar, S. C. N. Montoya, J. L. Cabrera and V. A. Rivarola, *Phytomedicine*, 2011, **18**, 1093.
- 49 (a) F. Ménard, V. Sol, C. Ringot, R. Granet, S. Alves, C. L. Morvan, Y. Queneau, N. Ono and P. Krausz, *Bioorg. Med. Chem.*, 2009, **17**, 7647; (b) I. Ott, K. Schmidt, B. Kircher, P. Schumacher, T. Wiglenda and R. Gust, *J. Med. Chem.*, 2005, **48**, 622.
- 50 (a) J. Michl, *J. Am. Chem. Soc.*, 1978, **100**, 6801; (b) J. Michl, *Tetrahedron*, 1984, **40**, 3845.
- 51 J. Mack, *Chem. Rev.*, 2017, **117**, 3444.
- 52 M. J. Frisch, *et al.*, Gaussian 09, see ESI for full reference.
- 53 Chemcraft - graphical software for visualization of quantum chemistry computations. <https://www.chemcraftprog.com>.